applied sciences

MDPI

Article

A Time-Interleave-Based Power Management System with Maximum Power Extraction and Health Protection Algorithm for Multiple Microbial Fuel Cells for Internet of Things Smart Nodes

Alfredo Costilla-Reyes [1,*], Celal Erbay [2], Salvador Carreon-Bautista [3], Arum Han [1] and Edgar Sánchez-Sinencio [1]

1 Department of Electrical and Computer Engineering, Texas A&M University, College Station, TX 77843-3128, USA; arum.han@ece.tamu.edu (A.H.); s-sanchez@tamu.edu (E.S.-S.)
2 TUBITAK-Informatics and Information Security Research Center, Kocaeli 41470, Turkey; celal.erbay@tubitak.gov.tr
3 Analog Devices, Colorado Springs, CO 80920, USA; Salvador.CarreonBautista@analog.com
* Correspondence: acostillar@tamu.edu; Tel.: +1-979-985-1351

Received: 25 October 2018; Accepted: 17 November 2018; Published: 27 November 2018

check for updates

Abstract: Microbial Fuel Cell (MFC) technology is a novel Energy Harvesting (EH) source that can transform organic substrates in wastewater into electricity through a bioelectrochemical process. However, its limited output power available per liter is in the range of a few milliwatts, which results very limited to be used by an Internet of Things (IoT) smart node that could require power in the order of hundreds of milliwatts when in full operation. One way to reach a usable power output is to connect several MFCs in series or parallel; nevertheless, the high output characteristic resistance of MFCs and differences in output voltage from multiple MFCs, dramatically worsens its power efficiency for both series and parallel arrangements. In this paper, a Power Management System (PMS) is proposed to allow maximum power harvesting from multiple MFCs while providing a regulated output voltage. To enable a more efficient and reliable power-harvesting process from multiple MFCs that considers the biochemical limitations of the bacteria to extend its lifetime, a power ranking and MFC health-protection algorithm using an interleaved EH operation was implemented in a PIC24F16KA102 microcontroller. A power extraction sub-block of the system includes an ultra-low-power BQ25505 step-up DC-DC converter, which integrates Maximum Power Point Tracking (MPPT) capabilities. The maximum efficiency measured of the PMS was ~50.7%. The energy harvesting technique presented in this work was tested to power an internet-enabled temperature-sensing smart node.

Keywords: DC-DC power conversion; Internet of Things (IoT); microbial fuel cell array; power management system; remote monitoring; step-up converter; wastewater

1. Introduction

It is projected that networked microsensor technology, in the form of Wireless Sensor Networks (WSNs), will keep playing an important role in the future of remote sensing [1]. Some of the applications for WSNs range from automation, human monitoring, equipment condition monitoring, defense, aerospace, building, structural health monitoring and agriculture [2–6].

As reported in [7], WSNs have been implemented in point-to-multipoint and local point-to-point communication networks achieving long-term field deployment but a limited sensing-data processing. However, WSNs are nowadays increasingly becoming part of a more pervasive concept, the Internet of

Things (IoT), which allows devices to communicate with each other and collect information on a much larger scale through the internet [8]. This opens new possibilities to achieve more comprehensive data processing of the information being collected. IoT has the potential to foster a large number of applications by enabling more devices to be connected to the web and make use of a wider range of pre-collected and pre-processed data.

A paramount challenge that can pose a limitation for a wider adoption in the use of IoT smart nodes in areas of difficult access, is inherently associated to its battery requirements for a considerable power specification needed to perform on-field sensor measurements and to send the collected information to the cloud. A desirable feature of WSN is to minimize not only the size and cost of the energy storage element itself, but also to reduce the maintenance needed to constantly replace the sensor's batteries. Harvesting enough energy from the environment where the WSN is physically located, can be a plausible solution to extend the battery life of a remote sensor and even fully power it for prolonged periods of time [9,10]. The sources of energy that can be harvested from the ambient include solar, kinetic, thermal gradient, radiofrequency, electromagnetic and Microbial Fuel Cells (MFCs) [11–16].

MFCs are a promising emerging source of energy harvesting that can transform organic and inorganic matter to generate electricity by using a bioelectrochemical conversion process [17–21]. MFCs can find a particular application in remote sensing [22] for places that are difficult to access routinely for maintenance but with abundant organic material available, such as sewage water and even oceans [23–25], where the use and replacement of batteries, can be costly or impractical [16,23,26–30]. A potential application that can combine IoT devices and MFC technologies is in the management and optimization of traditionally public services, such as residual water treatment plants [31]. It is important to note that while MFCs can generate power from liquid and organic sediments found in wastewater and oceans, smart nodes can monitor and transmit conditions found in water being treated, such as temperature, pH, conductivity, salinity, and organic sediment concentration, to name a few [23–25,32].

Despite these opportunities, one of the main limitations of energy harvesting from MFC technologies is the low output power levels provided by each individual cell, typically in the order of microwatts to a few milliwatts per liter [33]. For this reason, a Power Management System (PMS) is required to maximize the power conversion efficiency and increase the voltage and current level to the nominal power levels required by wireless sensors. Some implementations of PMS have previously been reported to maximize the energy harvesting efficiencies of single MFCs [23,28–30,34–36]. To reach usable output voltage levels while at the same time increasing the output current density is by connecting several MFCs in series or in parallel to increase the overall power out level. However, differences in power production from individual MFCs, as well as voltage reversal issues when connecting multiple MFCs in series, present a challenge in the overall efficiency of the system, since these variations dramatically worsen the power production of MFCs arrays [33].

The objective of this paper is to present a circuit topology for efficient energy harvesting from multiple MFCs to increase the total available energy of the system to meet the voltage and current specifications of a power-demanding application. A ranking algorithm was developed based not only on the voltage of the MFC, which does not contain information about MFCs internal resistance, but rather on the available power from each individual MFC to prioritize the charge extraction from the MFC that has the highest available power. At the same time, recovery time is a critical observed requirement for the MFC to recharge its internal capacitive elements as part of its power generation cycle, to avoid damaging the MFC, due to power over-depletion and extend its lifetime. The algorithm also includes an MFC-failure protection feature that isolates an MFC in the array when the algorithm notices a significant power drop during the energy harvesting process. The MFC output power is regulated by a step-up DC-DC converter that stores the extracted charges in an output supercapacitor. Finally, the energy harvesting technique presented in this work is tested and demonstrated through an internet-enabled smart node, capable of transmitting the collected data to the internet. A performance comparison to other power management works based on MFC is made in terms of charging time, topology features and efficiency.

The paper is organized as follows: In Section 2, a brief introduction to MFC is presented and its electrical model is described. Section 3 discusses the choice of top level circuit architecture for multiple MFC power extraction and describes the MFC power ranking and power extraction algorithms. The experimental results are presented in Sections 4 and 5 summarizes this work.

2. MFC and Power Management System Specification

This section aims to provide accurate details of the construction of the MFCs used in this work, its electrical description to determine the proper PMS specifications and the proposed system specifications. All these components are described in the following.

2.1. MFC Construction and Characterization

Four MFCs were fabricated from an acrylic anode and cathode chambers. One 1000 mL MFC and three 240 mL MFCs were constructed, the two different sizes were used to simulate MFCs having different output power levels. A Proton Exchange Membrane (PEM) (Nafion 117^{TM}, Ion Power Inc., New Castle, DE, USA) was used to separate the anode and cathode chambers from each other, while selectively allowing proton generated by bacteria to cross over to the cathode chamber to complete the electrochemical reaction to produce power. The anode was a carbon felt (Morgan, Durham, CT, USA) and the cathode was a carbon cloth containing 0.5 mg/cm^2 of Pt catalyst on one side (ElectroChem, Inc., Woburn, MA, USA) for all MFCs. Both anode and cathode were connected through a titanium wire to a 1 kΩ load resistor that was placed between them to allow the electrons produced by bacteria to flow. The schematic diagram of the MFC is shown in Figure 1a. The electrical model in Figure 1b is further discussed in Section 2.2.

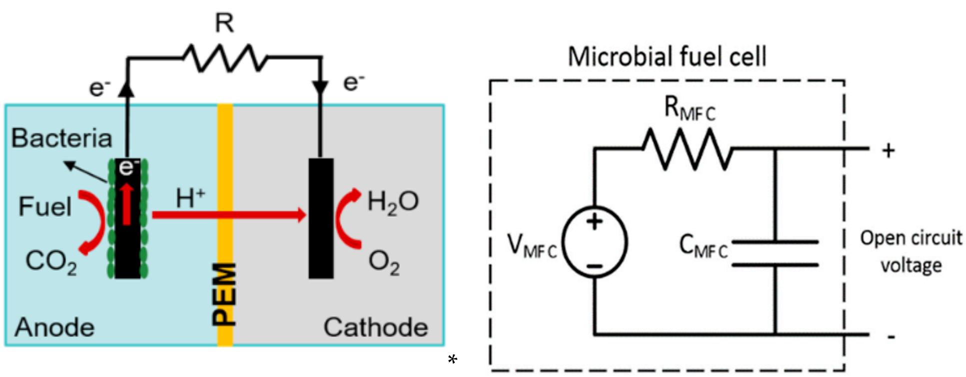

(**a**) (**b**)

Figure 1. Microbial Fuel Cell (MFC) device description (**a**) schematic and (**b**) electrical model.

All MFCs were inoculated with anaerobic activated sludge collected from the Austin Wastewater Treatment Plant for the initial growth of the bacteria on anodes. Then growth medium containing acetate (1.0 g/L) in Nutrient/Mineral/Buffer (NMB) solution was used (10 mL/L mineral base 1, 10 mL/L mineral base 2, and 1 mL/L nutrient base). The solution was replaced with a fresh one when the voltage across the load resistor dropped below 50 mV [28,37–39]. The constructed two-chamber MFCs are shown in Figure 2.

The MFC voltages were monitored in real time in volts (V) against time in seconds (s) [40] by using a digital multimeter (Fluke 79 series II, Everett, WA, USA) through a multiplexer (Agilent 34970A, Santa Clara, CA, USA). Once the voltage production level was stable, power and voltage at maximum power point were obtained by varying a testing load resistor value between the electrodes in the range of 5–20 Ω [41]. Table 1 summarizes the specifications and typical power production of all MFCs.

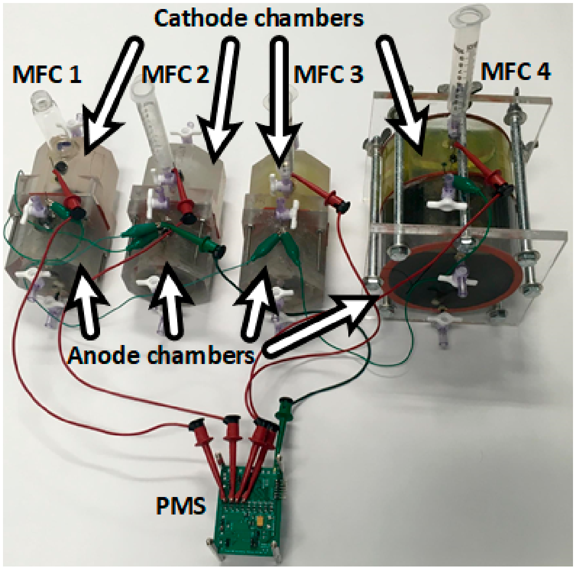

Figure 2. Two-chamber microbial fuel cell and power management unit set up.

Table 1. Specifications and performance of MFCs.

	MFC 1	MFC 2	MFC 3	MFC 4
Total volume (mL)	240	240	240	1000
Catholyte	Air	Air	Ferricyanide	Ferricyanide
Anode area (cm^2)	12	12	12	50
Cathode area (cm^2)	12	12	12	50
Power @ maximum power point (MPP) (µW)	595	484	435	6400

2.2. MFC Electrical Equivalent Modeling

The MFC can be electrically modeled as a voltage source with an internal resistance R_{MFC}, open circuit voltage V_{MFC}, and internal capacitance C_{MFC} as shown in Figure 1b. The value of R_{MFC} is composed of several different components (anode, cathode, membrane, and electrolyte resistances) [28–30]. The value of V_{MFC} is the MFC's thermodynamic voltage, which varies nonlinearly depending on the solution pH, temperature, and substrate concentration. Since MFCs produce a DC voltage, C_{MFC} is mostly ignored in similar works [16,27]. However, due to the method of locating the Maximum Power Point (MPP) through the open circuit voltage of the MFC in the proposed PMS, C_{MFC} is important for the proper design of a Maximum Power Point Tracking (MPPT) algorithm; thus, it is included in our model. The equivalent circuit model of the MFC was used for the design of the PMS and the dynamic MPPT in this work.

2.3. System Specifications

A voltage regulation stage is required to boost the low voltages (less than 1 volt) provided by each of the four MFCs to a nominal voltage that can provide proper power values for the wireless sensor to operate properly. The step-up converter integrated into the system provides dynamic impedance matching and low-power consumption for maximum-power extraction.

Since power extraction is performed to an array of four MFCs, MFC's health-state measurements, multiplexing control capabilities and the flexibility offered by a programmable device are key features required for the control block of the proposed system. Thus, an extremely-low power microcontroller is required to perform MFCs power ranking and multiplexing operations.

The energy-storage system requirements for an IoT smart node required the incorporation of an output load supercapacitor of 5 F, that can support 30 s of active temperature sampling and data transmission to the cloud, to meet the power specifications for an internet-enabled temperature sensor.

A super capacitor allows not only a larger charge storage as compared to standard capacitors, but also longer charging and discharging cycles than their lithium-ion battery counterparts. The design specifications are presented in Table 2.

Table 2. Specifications of the MFC-powered Internet of Things (IoT) system.

Specification	Value
Number of MFCs	4
Average Vin	350 mV
Vout	3.3 V
Output supercapacitor	5 F

3. Circuit Architecture for Multi-MFC PMS

In this section, a summary of previous EH techniques for multiple MFC is presented along with a proposed architecture that considers a DC-DC converter with MPP capabilities that has been tailored for MFC technology. A PMS algorithm has been embedded in a Programmable Intelligent Computer (PIC) microcontroller and explained here, its main purpose is to allow the extraction of an array of MFCs while providing health protection features. Finally, a description of the final implementation of the proposed PMS is given.

3.1. Overview of Energy Harvesting for MFC

Due to the technology's nature, the MFC output voltage is very low and non-regulated [28], which represents a major challenge for efficient power extraction. A parallel configuration of MFCs can be used to increase the output current with the disadvantage that the output voltage will remain at low levels. Another drawback of the parallel connection of MFCs is that if their output voltage deviates from each other, this effect leads to a detrimental charge transfer among cells in the array, also known as voltage reversal, preventing the stack of MFCs to fully deliver its charges to a load [26]. This results in power losses that lead to a low overall power efficiency of the array.

On the other hand, a serial connection of MFCs provides higher output voltages based on the sum of individual V_{MFC}, with a common current that flows throughout the MFC array. In [33] a voltage balancer is used along with a DC-DC converter for an array of serially connected MFCs. By doing so, the output voltage, now higher than that of a single MFC, is efficiently harvested by providing an active switching capacitor method to balance the system. However, the system can also face multiple drawbacks, including power extraction interruption, and even system failure if a single MFC in the stack is damaged or physically disconnected, due to a contact deterioration, for example. This can potentially disable the operation of the DC-DC converter block, leading to a loss of power available from the remaining properly-functioning MFCs.

Previous works in PMS have mainly focused on power extraction from a single MFC [27,42]. This approach is limited to the amount of power that a single MFC can generate, which can be depleted quickly, resulting in the interruption of the power supply at the load. In addition, if the system does not integrate an automatic MPPT algorithm, achieving maximum power harvesting can become cumbersome and time-consuming if conducted manually [23,27,33,43–45]. Even more important, power extraction may not be efficient, since the MPP can shift during the lifetime of an MFC. For this reason, the integration of an MPPT is essential for the DC-DC converter to dynamically adjust to the electrical characteristics across multiple MFCs.

In this work, the system proposed is intended to harvest the energy from an array of MFCs in a time interleaved fashion, allowing the inactive MFCs to recharge its internal capacitances (C_{MFC}) when they are not being harvested. The system also integrates an MFC-failure protection mechanism, which automatically isolates one or multiple MFCs from the system if its available power is below a minimum threshold. The MFC-failure protection feature is intended to isolate an MFC when it has been depleted, damaged or it has been physically disconnected.

3.2. Overview of the Proposed PMS Circuit for Multi-MFC

The block diagram of the proposed system is shown in Figure 3. Each MFC in the array is individually connected to a low-R_{on} N-type CMOS switch DMN1019UVT (Diodes Incorporated®, Plano, TX, USA), controlled by an extremely low power microcontroller PIC24F16KA102 (Microchip Technology Inc.®, Chandler, AZ, USA) [46]. The PMS algorithm embedded in the microcontroller allows testing the total power available in each MFC in the array, by using a power measurement block, as shown in Figure 4. The microcontroller also regulates the power extracted from an individual MFC in the stack by defining the time interleaved EH sequence and the amount of time needed for each MFC before it is harvested again. The DC-DC converter block consists of an ultra-low power boost converter BQ25505 (Texas Instruments Incorporated®, Dallas, TX, USA) [47]. Finally, the extracted charges are stored in an output supercapacitor that powers the IoT sensor.

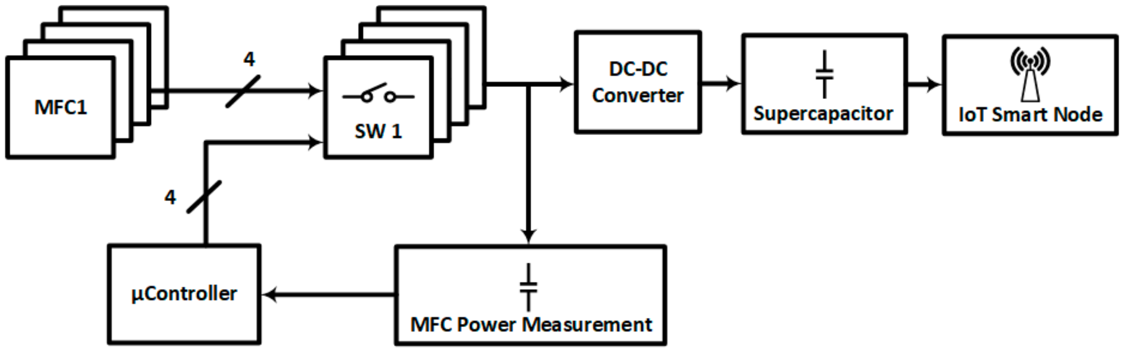

Figure 3. Block diagram of the proposed Power Management System (PMS).

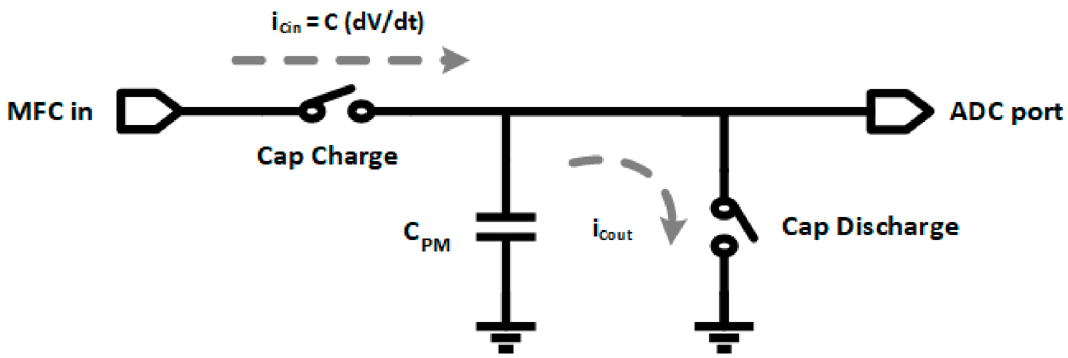

Figure 4. Diagram of the proposed power measurement circuit.

As the output voltage level of the MFC is not high enough for the proposed topology to allow for self-starting operation from the PMS, an external one-time pre-charging of an output secondary capacitor to 1.8 V is required to begin controller operation. Multiple different approaches may be taken to startup the system [48,49].

Once the system begins extracting energy from the MFC, there is no longer need for an external power source to power the PMS.

3.3. Maximum Power Point DC-DC Converter

Based on the electrical diagram presented in Figure 1b, the DC-DC boost converter selected for this work was programmed to set its input resistance at 50% of the V_{MFC} open circuit voltage [29]. As shown in Equation (1), since the maximum power point is reached when the input resistance of the PMS equals to the MFC's input resistance characteristic, it sets a minimum condition for the power losses that can be tolerated in by the internal resistance of switches, and sheet resistance for the Printed Circuit Board (PCB).

$$\begin{gathered} P_{LOSS} = I^2 R_{LOSS};\ R_{LOSS} = R_{MFC} \\ \Rightarrow R_{PMU+PCB} \leq R_{MFC}. \end{gathered} \tag{1}$$

3.4. Multi-MFC PMS Algorithm

A microcontroller's 10-bit Analog to Digital Converter (ADC) determines the interleaved power extraction time per MFC. As seen in Figure 5, the algorithm defines two thresholds for the power extraction $V_{th-High}$ and V_{th-Low} as follows:

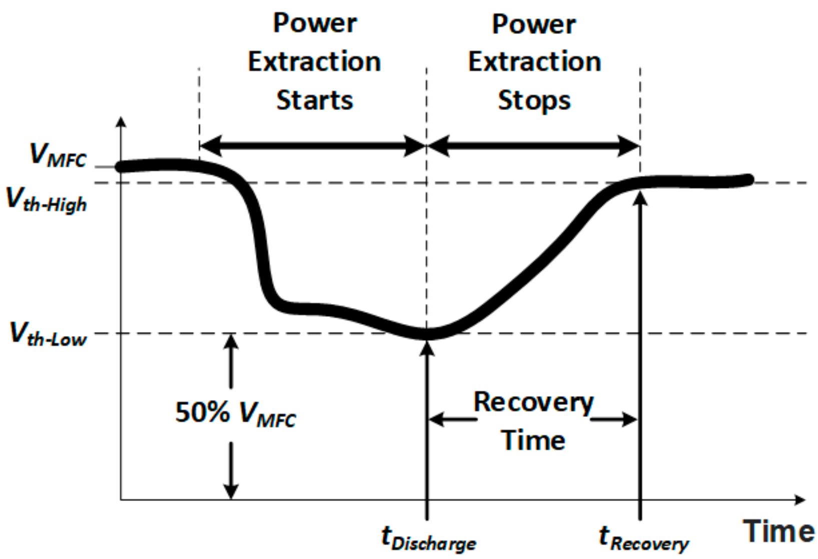

Figure 5. Key algorithm reference points of MFC power extraction waveform.

V_{th-Low} determines when to stop the EH operation and is predefined at 50% of the initial measured V_{MFC}. When V_{th-Low} is reached, the MFC is removed from the PMS until the voltage threshold high, $V_{th-High}$, is reached. The recovery time is defined as the time it takes for the MFC to go from V_{th-Low} to $V_{th-High}$. V_{th-Low} and $V_{th-High}$ are determined after selecting the voltage thresholds that yield the most optimum power extraction and recovery time for energy harvesting, without over-depleting the MFC from a series of threshold testing of an adaptive algorithm.

The power extraction algorithm presented in Figure 6a is described below:

1. The Power Ranking Algorithm subroutine (described in Section 3.5) is executed. As a return variable, a look-up table is filled out with the individual MFCs' power rankings
2. The look-up table is accessed to interleave the MFC power extraction process
3. The DC-DC boost converter is enabled to start EH
4. V_{MFC} is compared to the low threshold voltage V_{th-Low}
5. When V_{th-Low} voltage is reached the DC-DC converter is disabled
6. If more MFCs in the array are waiting to be harvested, then the program jumps to instruction #2. Otherwise, the system stops its EH mode and waits until the recovery time of the highest ranked MFC is reached
7. After the recovery time is completed, the algorithm restarts.

The proposed interleaved energy extraction allows the step-up DC-DC converter to dynamically find the MPP of each individual MFC, ensuring a maximum power output per MFC while at the same time, the idle time for the remaining MFCs is used as an MFC's recovery time that directly affects the MFC's health status.

Another important feature of this approach is that if there is a failure at one or more MFCs, the system automatically adapts to it by assigning a rank of zero to that specific MFC, which allows the system to neglect the damaged cell.

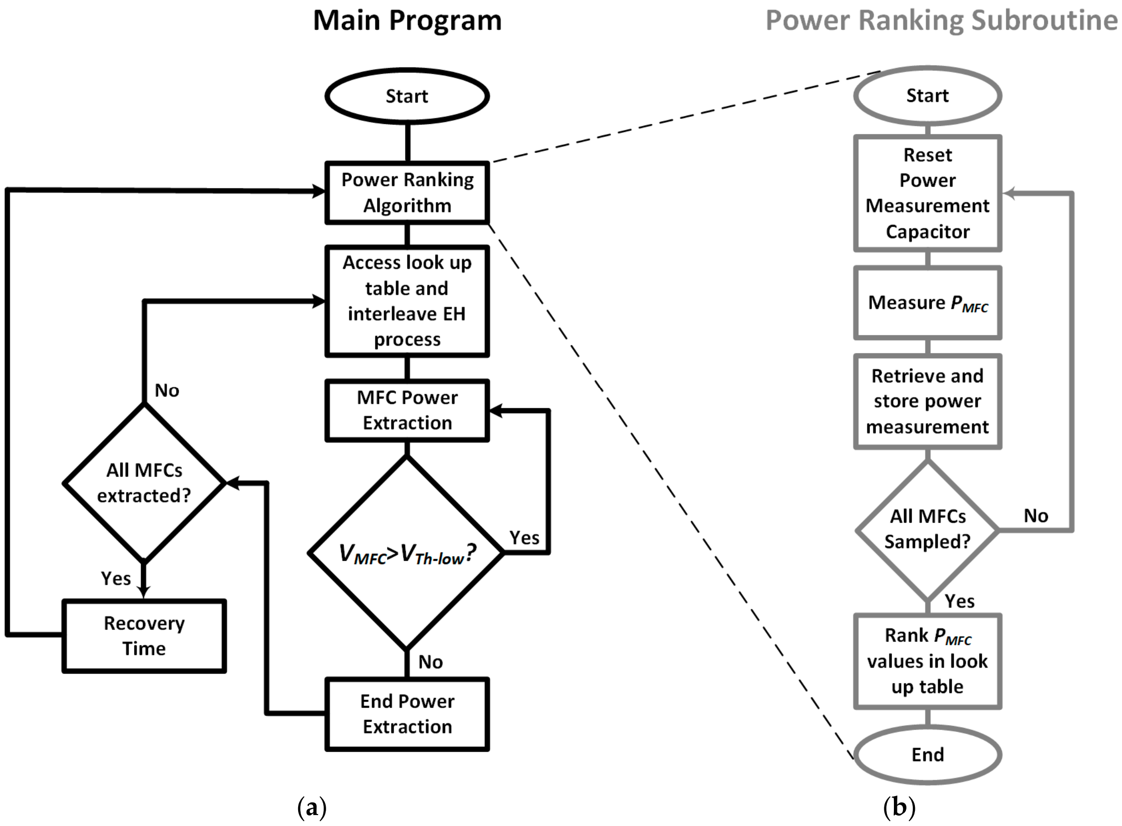

Figure 6. Flow diagram for MFC power extraction: (**a**) Main Program and (**b**) Power Ranking Algorithm subroutine.

3.5. Power Ranking from Multiple MFCs

Due to the bioelectrochemical nature of the MFC (parasitic reactive elements), its open circuit output voltage does not hold a direct relationship to the total amount of energy. Measuring the MFC open circuit output voltage it is not necessarily indicative of the amount of energy available from a specific device in the array because its internal resistance (R_{MFC}) is not considered. Therefore, the followed approach was chosen to properly estimate the power available per MFC:

The circuit shown in Figure 4 uses a 100 µF power measurement capacitor (C_{PM}) and a charging switch (Cap Charge) in a series to an MFC under testing. A second switch (Cap Discharge) is in parallel with C_{PM} to reset its voltage conditions at the end of a power measurement by setting its initial voltage to zero. By neglecting parasitic elements, the power in the circuit shown in Figure 4 can be calculated using Equation (2) below:

$$P = V \cdot I = V(t) \cdot C_{PM} \frac{dV}{dt}. \quad (2)$$

It can be noticed from Equation (2) that the voltage change in time $\frac{dV}{dt}$ of C_{PM} is directly proportional to the total available power of the MFC under test, and most importantly, such as charging time, as estimated in Equation (3), intrinsically considers resistances R_{MFC} and R_{Switch}, where the latter resistance is constant. Using this principle, the power ranking algorithm registers an accurate power measurement every 16.52 ms.

$$\tau_{Discharge} = C_{MFC} \cdot R_{out} = C_{MFC} \cdot (R_{MFC} + R_{Switch}). \quad (3)$$

Thus, the final value of C_{PM}, holds a direct relationship to the MFC's individual power. Both, the capacitor value and the constant charging time were selected to provide meaningful information regarding the electrical characteristics of all the MFCs connected to the system. The previously described process is repeated for each MFCs located in the MFC array. After all the MFCs are measured, the data is sorted in a look-up table that mandates the order in which each MFC is harvested.

The description of the power ranking sub-routine shown in Figure 6b is presented below:

1. The power ranking measurement capacitor is initialized to 0 V by Cap Discharge switch
2. The MFC under testing is connected to the ranking circuit using Cap Charge switch
3. ADC values of MFC measured power are stored in the look-up table
4. The ADC values are sorted, assigning the highest rank to the MFC with maximum voltage, and lowest rank to the MFC with minimum voltage. MFCs that cannot provide significant power are ranked zero and neglected in the subsequent EH process.

3.6. Implementation

The proposed PMS was developed on a two-layer PCB shown in Figure 7. On the top side, a microcontroller was placed along with the low-R switches and the power measurement capacitor. The DC-DC boost converter is found at the bottom side of the PCB. Detailed files of this work can be found in the Supplementary Materials section of this manuscript.

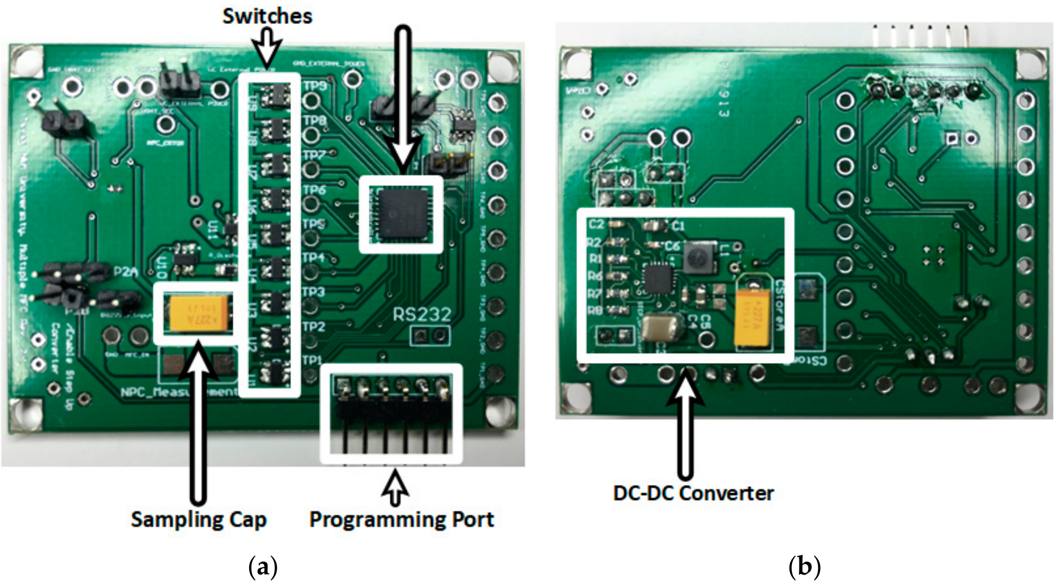

Figure 7. Printed Circuit Board of the PMS for multi-MFC power extraction, (**a**) top view; (**b**) bottom view.

The collected power is stored in an off-board output supercapacitor that powers the IoT sensor node used to test the system.

The final algorithm was implemented using MPLAB X IDE and XC8 programmed in the PIC24F16KA102's non-volatile internal flash memory. It is important to mention that even though the information retrieved by the power ranking algorithm was stored in the volatile data memory, the use of a non-volatile Electrically Erasable Programmable Read-Only Memory (EEPROM) to store such power ranking values is available in case further off-line data analysis is required. The sensor data collected in this work is acquired with the purpose to be transmitted and stored in a remote server in the cloud to enable further and more complex data analysis.

Even though the proposed system can natively support up to nine MFC devices without any further modification only four MFCs were tested in this work. It is also important to notice that if more

MFCs are needed to increase the overall power available, the system can easily be adapted by adding more solid-state switches and digital multiplexers as needed.

4. Experimental Results and Discussion

4.1. PMS for Multiple MFCs

The operation of the power ranking subroutine operation is illustrated in Figure 8, which displays the C_{PM} output voltage. The label Sample 1–4, indicate when the respective MFC 1–4 is power-measured by sampling its output power using C_{PM} such value is held to perform an analog-to-digital conversion. This sampling process is repeated for each MFC connected to the board periodically and its ranking values are grouped in phases. The ranking obtained at the phase is shown in Table 3, phase one. After the MFCs are sorted, then the power extraction can be performed. Phase two in Table 3, represents a second power-ranking measurement recalibration.

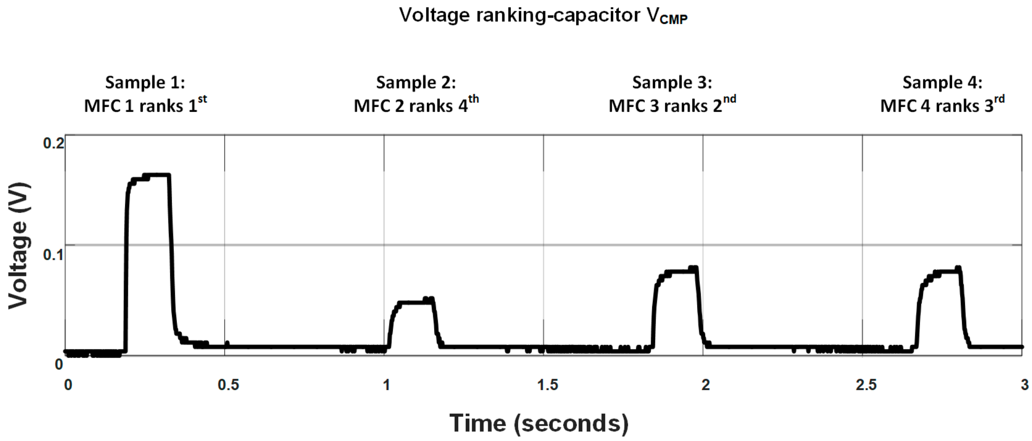

Figure 8. MFC power ranking waveform.

Table 3. MFC power rank.

Device	Ranking (Phase One)	Ranking (Phase Two)
MFC 1	1st	1st
MFC 2	4th	2nd
MFC 3	2nd	3rd
MFC 4	3rd	4th

In Figure 9, the time interleaved power extraction operation of the proposed PMS is presented for different extraction phases. The four channels representing the MFC output voltages are labeled at the top of the graph. Initially, before power extraction, the voltage at the MFC represents its open circuit voltage; then, when the MFC is harvested its voltage drops to its MPP voltage. Finally, when V_{th-Low} is reached, the algorithm harvests the next MFC in the look-up table only if its output voltage is larger than $V_{th-High}$.

Figure 9a shows the energy harvesting operation right after performing the MFC power ranking presented in Figure 8. Thus, the pattern for the power extraction, pointed out with gray arrows, follows the pattern described in Table 3 for phase one; however, after extracting power from the MFCs for ~20 h, the MFCs' power ranking look-up table recalibrates to the values shown in Table 3, phase two. Such power changes are illustrated in Figure 9b. It is important to highlight that, in phase two, not only are the power rankings changed for devices MFC 2, MFC 3, and MFC 4, but at this point MFC 1 now takes more time to reach $V_{th-High}$. This condition forces the algorithm to switch to the next available MFC that complies with the $V_{th-High}$ specifications, which in this case is MFC 2. The algorithm continues its operation, and MFC 1 is only harvested again when $V_{th-High}$ is reached as originally proposed.

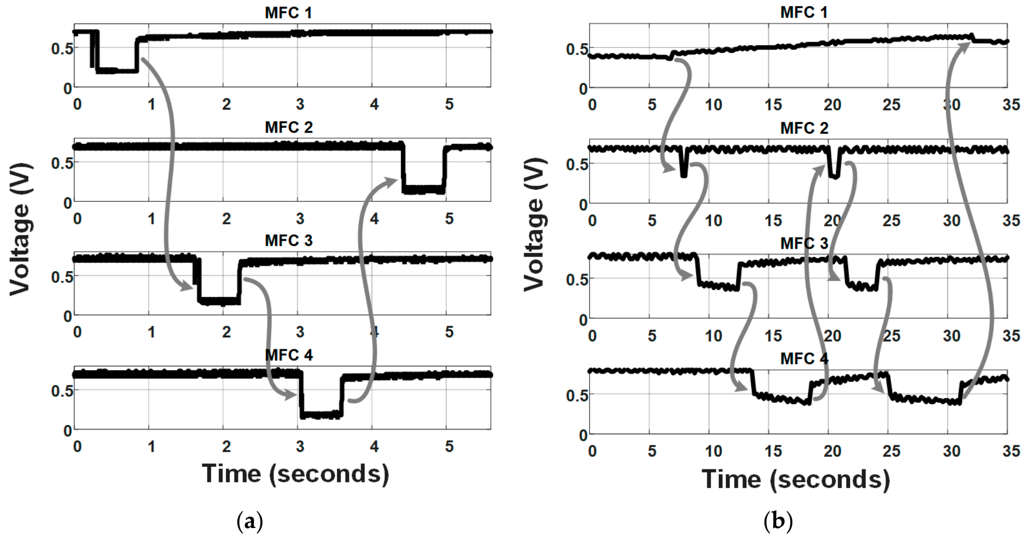

Figure 9. MFC interleaved power extraction measurements: (**a**) Phase one and (**b**) phase two.

As demonstrated, an important characteristic of the power ranking feature previously demonstrated, is that if an MFC does not provide proper power conditions or has an internal failure, the system automatically isolates the damaged MFC and continues its operation without affecting the remaining MFCs or interrupting the energy harvesting process.

4.2. IoT Sensor Node Application

An IoT application was implemented to test the capabilities of the proposed PMS for a power demanding extraction conditions. A Wi-Fi-enabled temperature smart node was designed and built for this purpose. This sensor node was based on the IoT platform Photon (Particle®, San Francisco, CA, USA) [50]. As seen in Figure 10a, the IoT circuit board was wirelessly connected to a router to send the collected data over the internet, and the information gathered was retrieved using a handheld iPhone® device. Figure 10b shows that the 5 F output supercapacitor was charged from 0 V to 3.3 V with an initial charging time (t_i) of 11.3 h; at 3.3 V the internet-enabled smart node was enabled, and the data was transmitted wirelessly to a remote server. After the data packet was received in the smartphone, the sensor was disconnected and the output capacitor voltage presented an output voltage of 2.8 V. It took an average recharging time (t_r) of three hours to fully recharge the supercapacitor from 2.8 V to 3.3 V. The process was repeated six times in the span of 24 h. The collected temperature readings are shown in Figure 10c.

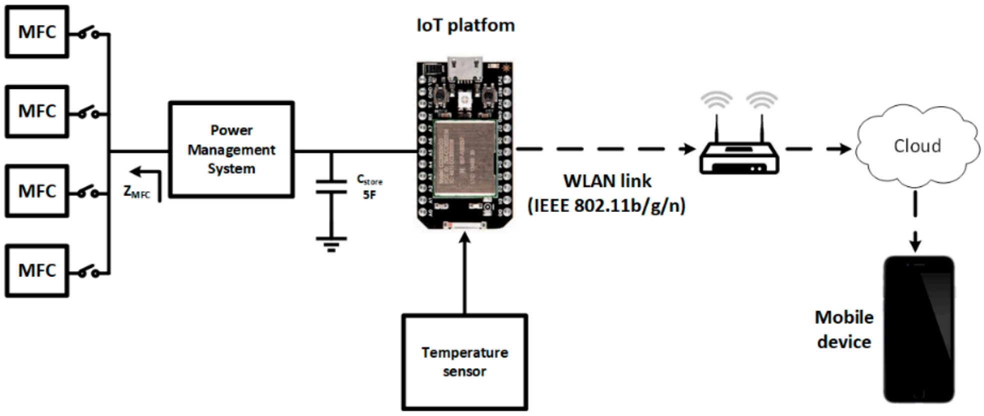

(**a**)

Figure 10. *Cont.*

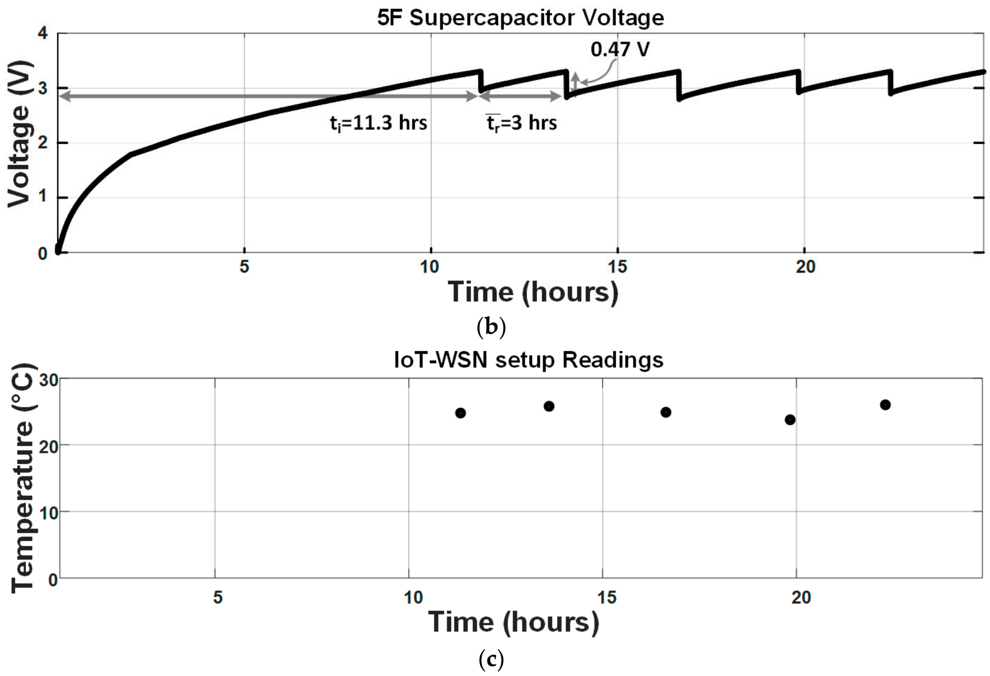

Figure 10. Internet of things sensor node. (**a**) Hardware setup; (**b**) supercapacitor voltage waveform and (**c**) temperature measurements.

By effectively powering the IoT application with the MFC array, the system robustness was confirmed after providing continuous power extraction in the span of 24 h, in such period the MFC did not show any abnormal stress or failure, validating in this way the potential use of MFC technology for power-hungry systems, such as IoT-applications.

4.3. Total Power Consumption and Efficiency

The PMS' power efficiency (η), as defined in (4), is presented in Figure 11. The peak end-to-end efficiency measured was ~50.7% for a 3.3 output voltage. Table 4 summarizes and compares the presented work to previously reported systems.

$$\eta = \frac{P_{out}}{P_{in}} \times 100 = \frac{P_{MFC} - \sum P_{losses}}{P_{MFC}} \times 100 \approx \frac{P_{MFC} - [I_{out}(R_{MFC} + R_{switch}) + P_{Loss_{Converter}}]}{P_{MFC}} \times 100. \quad (4)$$

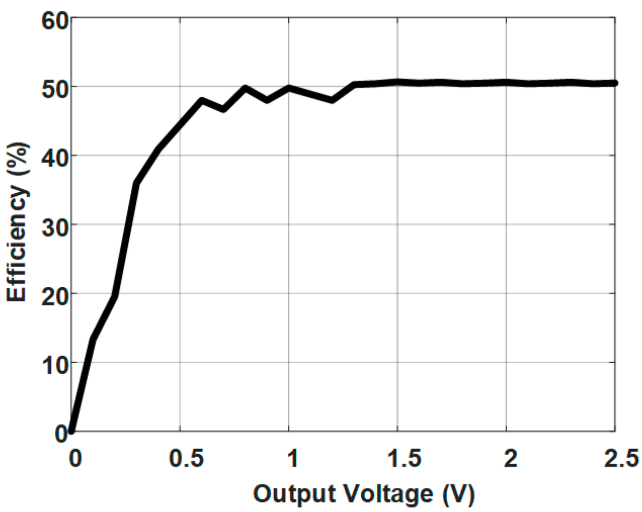

Figure 11. Measured Efficiency versus Output Voltage.

Table 4. Comparison of MFC power management units.

Specification	[51]	[27]	[29]	[28]	[33]	[52]	This Work
Input voltage	300 mV	300 mV	300–720 mV	300–600 mV	1.4 V (DC-DC converter input)	300 mV	330 mV
Output voltage	1 V	1.8 V	2.5 V	2.5 V	4.25 V	3.3 V	3.3 V
Inductor	326.7 µH	2 µH	1.5 mH	1.5 mH	Transformer 31.8 mH (primary winding)	-	22 µH
Output capacitor	8 µF	47 µF	0.1 F (supercapacitor)	0.1 F	68 mF	Multiple	5 F
Maximum power extraction	-	-	Adaptable Maximum Power Extraction	Yes	MPPT	-	MPPT
Efficiency	73%	-	58%	30%	-	35.02%	50.7%
Implementation approach	Discrete Components	Discrete Components	Custom integrated circuit	Custom integrated circuit	Discrete Components	Discrete Components	Discrete Components
Multiple MFC power extraction	No	No	No	No	Yes	Multi anode	Yes (default support for 9 MFCs)
MFC health protection	-	-	-	-	No	No	Yes

5. Conclusions

This paper presents a system design that can extract power from an array of MFCs using a time-interleave technique that not only enables a custom MPPT per MFC in the arrange but also allows a proper MFC charge-recovery time to avoid overly depleting the cells in the array, which can lead to an MFC failure or premature end-of-life. An optimal power harvesting process was measured when enabling a maximum power point tracking in the DC-DC power conversion block across four different MFCs with an output characteristic power at MPPT ranging from 6400 µW to 435 µW with an observed 50.7% peak efficiency. The results of the proposed system show a robust performance of the proposed PMS after more than 24-h of MFC EH.

The system was able to run autonomously to charge an output supercapacitor of 5 F from 0 V to 3.3 V in 13.6 h and endure a 24-h power extraction with no signs of MFC over-depletion or failure. The system powered an internet-enabled smart node five times, and the information was correctly retrieved from a remote server using a smartphone device.

By successfully completing this MFC-powered IoT-sensor node demonstration, EH based on MFC technology has been verified as a promising area that has the capabilities to run power intense systems, such as internet-enabled technologies, which can potentially enable the arrival of a new generation of self-powered smart nodes.

Finally, future work in this area includes the development of efficient PMS startup circuits tailored to MFC technology, more efficient low-power data acquisition and processing techniques for remote sensing, in which the addition of new sensors and analytical models in the cloud can give accurate real-time and predictive information about the health state of the MFC.

Supplementary Materials: The following are available online at www.mdpi.com/2076-3417/8/12/2404/s1, File S1: source code and circuit schematics of this work, applsci-386823.

Author Contributions: A.C.-R. is the main author and thus responsible for writing the paper. C.E. has contributed to Section 2.1 and by providing MFC devices, equipment, laboratory space and materials, S.C.-B. contributed to Section 3.3 and industry insight in the area of power management systems. A.H. and E.S.-S. have been responsible for revising and supervising the paper in the MFC side and the electronics circuits aspects, respectively. Conceptualization: A.C.-R. and S.C.-B.; Data curation, A.C.-R.; Funding acquisition, A.H. and E.S.-S.; Investigation, A.C.-R.; Project administration, E.S.-S.; Resources, A.H. and E.S.-S.; Software, A.C.-R.; Supervision, A.H. and E.S.-S.; Validation, C.E.; Writing—review and editing, A.C.-R., C.E. and S.C.-B.

Funding: This research was partially funded by the Qatar National Research Foundation (QNRF), grant number #NPRP 7-1634-2-604

Acknowledgments: This work was supported by Consejo Nacional de Ciencia y Tecnología (Mexico City, Mexico), Texas Instruments (Dallas, TX, USA), Silicon Labs (Austin, TX, USA) and Intel (Hillsboro, OR, USA).

Conflicts of Interest: The authors declare no conflict of interest.

References

1. Chong, C.Y.; Kumar, S.P. Sensor networks: Evolution, opportunities, and challenges. *Proc. IEEE* **2003**, *91*, 1247–1256. (In English) [CrossRef]
2. Gèungèor, V.ð.; Hancke, G.P. *Industrial wireless Sensor Networks: Applications, Protocols, And Standards*; (Industrial Electronics Series), PP. 1 Online Resource (xxxii, 374 Pages); CRC Press: Boca Raton, FL, USA, 2017.
3. Tiwari, A.; Lewis, F.L.; Ge, S.S. Wireless sensor network for machine condition based maintenance. In Proceedings of the 2004 8th Control, Automation, Robotics and Vision Conference, Kunming, China, 6–9 December 2004; pp. 461–467. (In English)
4. Swartz, R.A.; Lynch, J.P.; Zerbst, S.; Sweetman, B.; Rolfes, R. Structural monitoring of wind turbines using wireless sensor networks. *Smart Struct Syst.* **2010**, *6*, 183–196. (In English) [CrossRef]
5. Konstantopoulos, C.; Koutroulis, E.; Mitianoudis, N.; Bletsas, A. Converting a Plant to a Battery and Wireless Sensor with Scatter Radio and Ultra-Low Cost. *IEEE Trans. Instrum. Meas.* **2016**, *65*, 388–398. (In English) [CrossRef]
6. Toh, W.Y.; Tan, Y.K.; Koh, W.S.; Siek, L. Autonomous Wearable Sensor Nodes with Flexible Energy Harvesting. *IEEE Sens. J.* **2014**, *14*, 2299–2306. (In English) [CrossRef]
7. Wang, Y.; Lynch, J.P.; Law, K.H. Design of a low-power wireless structural monitoring system for collaborative computational algorithms. *Proc. Soc. Photo-Opt. Instrum.* **2005**, *5768*, 106–117. (In English)
8. Atzori, L.; Iera, A.; Morabito, G. The Internet of Things: A survey. *Comput. Netw.* **2018**, *54*, 2787–2805. (In English) [CrossRef]
9. Seah, W.K.; Tan, Y.; Chan, A.T. Research in energy harvesting wireless sensor networks and the challenges ahead. In *Autonomous Sensor Networks*; Springer: Berlin, Germany, 2012; pp. 73–93.
10. Wan, Z.G.; Tan, Y.K.; Yuen, C. Review on energy harvesting and energy management for sustainable wireless sensor networks. In Proceedings of the 2011 IEEE 13th International Conference on Communication Technology, Jinan, China, 25–28 September 2011; pp. 362–367.
11. Raghunathan, V.; Kansal, A.; Hsu, J.; Friedman, J.; Srivastava, M. Design considerations for solar energy harvesting wireless embedded systems. In Proceedings of the Fourth International Symposium on Information Processing in Sensor Networks, Boise, ID, USA, 15 April 2005; pp. 457–462. (In English)
12. Zarate-Roldan, J.; Carreon-Bautista, S.; Costilla-Reyes, A.; Sanchez-Sinencio, E. A Power Management Unit With 40 dB Switching-Noise-Suppression for a Thermal Harvesting Array. *IEEE Trans. Circuits Syst. I Reg. Pap.* **2015**, *62*, 1918–1928. (In English) [CrossRef]
13. Calhoun, B.H.; Daly, D.C.; Verma, N.; Finchelstein, D.F.; Wentzloff, D.D.; Wang, A.; Cho, S.-H.; Chandrakasan, A.P. Design considerations for ultra-low energy wireless microsensor nodes. *IEEE Trans Comput.* **2005**, *54*, 727–740. (In English) [CrossRef]
14. Vullers, R.J.M.; Schaijk, R.v.; Visser, H.J.; Penders, J.; Hoof, C.V. Energy Harvesting for Autonomous Wireless Sensor Networks. *IEEE Solid-State Circuits Mag.* **2010**, *2*, 29–38. [CrossRef]
15. Moghe, R.; Yang, Y.; Lambert, F.; Divan, D. A Scoping Study of Electric and Magnetic Field Energy Harvesting for Wireless Sensor Networks in Power System Applications. In Proceedings of the 2009 IEEE Energy Conversion Congress and Exposition, San Jose, CA, USA, 20–24 September 2009; Volumes 1–6, pp. 3423–3430. (In English)
16. Wang, H.M.; Park, J.D.; Ren, Z.Y. Active Energy Harvesting from Microbial Fuel Cells at the Maximum Power Point without Using Resistors. *Environ. Sci. Technol.* **2012**, *46*, 5247–5252. (In English) [CrossRef] [PubMed]
17. Logan, B.E.; Hamelers, B.; Rozendal, R.; Schröder, U.; Keller, J.; Freguia, S.; Aelterman, P.; Verstraete, W.; Rabaey, K. Microbial fuel cells: Methodology and technology. *Environ. Sci. Technol.* **2006**, *40*, 5181–5192. (In English) [CrossRef] [PubMed]
18. Lovley, D.R. The microbe electric: Conversion of organic matter to electricity. *Curr. Opin. Biotech.* **2008**, *19*, 564–571. (In English) [CrossRef] [PubMed]

19. He, Z.; Minteer, S.D.; Angenent, L.T. Electricity generation from artificial wastewater using an upflow microbial fuel cell. *Environ. Sci. Technol.* **2005**, *39*, 5262–5267. (In English) [CrossRef] [PubMed]
20. Logan, B.E. Exoelectrogenic bacteria that power microbial fuel cells. *Nat. Rev. Micro.* **2009**, *7*, 375–381. [CrossRef] [PubMed]
21. Pant, D.; van Bogaert, G.; Diels, L.; Vanbroekhoven, K. A review of the substrates used in microbial fuel cells (MFCs) for sustainable energy production. *Bioresour. Technol.* **2010**, *101*, 1533–1543. [CrossRef] [PubMed]
22. Ivars-Barcelo, F.; Zuliani, A.; Fallah, M.; Mashkour, M.; Rahimnejad, M.; Luque, R. Novel Applications of Microbial Fuel Cells in Sensors and Biosensors. *Appl. Sci.* **2018**, *8*, 1184. [CrossRef]
23. Donovan, C.; Dewan, A.; Heo, D.; Beyenal, H. Batteryless, Wireless Sensor Powered by a Sediment Microbial Fuel Cell. *Environ. Sci. Technol.* **2008**, *42*, 8591–8596. (In English) [CrossRef] [PubMed]
24. Tender, L.M.; Gray, S.A.; Groveman, E.; Lowy, D.A.; Kauffman, P.; Melhado, J.; Tyce, R.C.; Flynn, D.; Petrecca, R.; Dobarro, J. The first demonstration of a microbial fuel cell as a viable power supply: Powering a meteorological buoy. *J. Power Sources* **2008**, *179*, 571–575. (In English) [CrossRef]
25. Bond, D.R.; Holmes, D.E.; Tender, L.M.; Lovley, D.R. Electrode-reducing microorganisms that harvest energy from marine sediments. *Science* **2002**, *295*, 483–485. (In English) [CrossRef] [PubMed]
26. Park, J.D.; Ren, Z. Hysteresis-Controller-Based Energy Harvesting Scheme for Microbial Fuel Cells with Parallel Operation Capability. *IEEE Trans. Energy Convers.* **2012**, *27*, 715–724. [CrossRef]
27. Meehan, A.; Gao, H.; Lewandowski, Z. Energy Harvesting with Microbial Fuel Cell and Power Management System. *IEEE Trans. Power Electron.* **2011**, *26*, 176–181. [CrossRef]
28. Erbay, C.; Carreon-Bautista, S.; Sanchez-Sinencio, E.; Han, A. High Performance Monolithic Power Management System with Dynamic Maximum Power Point Tracking for Microbial Fuel Cells. *Environ. Sci. Technol.* **2014**, *48*, 13992–13999. (In English) [CrossRef] [PubMed]
29. Carreon-Bautista, S.; Erbay, C.; Han, A.; Sanchez-Sinencio, E. Power Management System with Integrated Maximum Power Extraction Algorithm for Microbial Fuel Cells. *IEEE Trans. Energy Convers.* **2015**, *30*, 262–272. (In English) [CrossRef]
30. Carreon-Bautista, S.; Erbay, C.; Han, A.; Sanchez-Sinencio, E. An Inductorless DC-DC Converter for an Energy Aware Power Management Unit Aimed at Microbial Fuel Cell Arrays. *IEEE J. Emerg. Sel. Top. Power Electron.* **2015**, *3*, 1109–1121. (In English) [CrossRef]
31. Zanella, A.; Bui, N.; Castellani, A.; Vangelista, L.; Zorzi, M. Internet of Things for Smart Cities. *IEEE Int. Things* **2014**, *1*, 22–32. (In English) [CrossRef]
32. Lee, I.; Kim, G.; Bang, S.; Wolfe, A.; Bell, R.; Jeong, S.; Kim, Y.; Kagan, J.; Arias-Thode, M.; Chadwick, B.; et al. System-On-Mud: Ultra-Low Power Oceanic Sensing Platform Powered by Small-Scale Benthic Microbial Fuel Cells. *IEEE Trans. Circuits Syst. I Reg. Pap.* **2015**, *62*, 1126–1135. (In English) [CrossRef]
33. Khaled, F.; Ondel, O.; Allard, B. Optimal Energy Harvesting from Serially Connected Microbial Fuel Cells. *IEEE Trans. Ind. Electron.* **2015**, *62*, 3508–3515. (In English) [CrossRef]
34. Shantaram, A.; Beyenal, H.; Raajan, R.; Veluchamy, A.; Lewandowski, Z. Wireless sensors powered by microbial fuel cells. *Environ. Sci. Technol.* **2005**, *39*, 5037–5042. (In English) [CrossRef] [PubMed]
35. Dallago, E.; Barnabei, A.L.; Liberale, A.; Torelli, G.; Venchi, G. A 300-mV Low-Power Management System for Energy Harvesting Applications. *IEEE Trans. Power Electron.* **2016**, *31*, 2273–2281. (In English) [CrossRef]
36. Plekhanova, Y.; Tarasov, S.; Kolesov, V.; Kuznetsova, I.; Signore, M.; Quaranta, F.; Reshetilov, A. Effects of Polymer Matrices and Carbon Nanotubes on the Generation of Electric Energy in a Microbial Fuel Cell. *Membranes (Basel)* **2018**, *8*, 99. [CrossRef] [PubMed]
37. Yang, G.; Erbay, C.; Yi, S.; de Figueiredo, P.; Sadr, R.; Han, A.; Yu, C. Bifunctional nano-sponges serving as non-precious metal catalysts and self-standing cathodes for high performance fuel cell applications. *Nano Energy* **2016**, *22*, 607–614. [CrossRef]
38. Erbay, C.; Pu, X.; Choi, W.; Choi, M.; Ryu, Y.; Hou, H.; Lin, F.; de Figueiredo, P.; Yu, C.; Han, A. Control of geometrical properties of carbon nanotube electrodes towards high-performance microbial fuel cells. *J. Power Sources* **2015**, *280*, 347–354. [CrossRef]
39. Erbay, C.; Yang, G.; de Figueiredo, P.; Sadr, R.; Yu, C.; Han, A. Three-dimensional porous carbon nanotube sponges for high-performance anodes of microbial fuel cells. *J. Power Sources* **2015**, *298*, 177–183. [CrossRef]
40. You, J.; Greenman, J.; Ieropoulos, I. Novel Analytical Microbial Fuel Cell Design for Rapid in Situ Optimisation of Dilution Rate and Substrate Supply Rate, by Flow, Volume Control and Anode Placement. *Energies* **2018**, *11*, 2377. [CrossRef]

41. Lin, H.; Wu, S.; Zhu, J. Modeling Power Generation and Energy Efficiencies in Air-Cathode Microbial Fuel Cells Based on Freter Equations. *Appl. Sci.* **2018**, *8*, 1983. [CrossRef]
42. Zhang, X.; Ren, H.; Pyo, S.; Lee, J.I.; Kim, J.; Chae, J. A High-Efficiency DC-DC Boost Converter for a Miniaturized Microbial Fuel Cell. *IEEE Trans. Power Electron.* **2015**, *30*, 2041–2049. [CrossRef]
43. Ren, Z.Y.; Ward, T.E.; Regan, J.M. Electricity production from cellulose in a microbial fuel cell using a defined binary culture. *Environ. Sci. Technol.* **2007**, *41*, 4781–4786. (In English) [CrossRef] [PubMed]
44. Aelterman, P.; Rabaey, K.; Pham, H.T.; Boon, N.; Verstraete, W. Continuous electricity generation at high voltages and currents using stacked microbial fuel cells. *Environ. Sci. Technol.* **2006**, *40*, 3388–3394. (In English) [CrossRef] [PubMed]
45. Dewan, A.; Beyenal, H.; Lewandowski, Z. Scaling up Microbial Fuel Cells. *Environ. Sci. Technol.* **2008**, *42*, 7643–7648. (In English) [CrossRef] [PubMed]
46. Microchip Technology Inc. PIC24F16KA102 Datasheet. Available online: www.microchip.com (accessed on 9 October 2011).
47. Texas Instruments. BQ25505 datasheet. Available online: www.ti.com (accessed on 28 August 2013).
48. Zhang, Y.; Zhang, F.; Shakhsheer, Y.; Silver, J.D.; Klinefelter, A.; Nagaraju, M.; Boley, J.; Pandey, J.; Shrivastava, A.; Carlson, E.J.; et al. A Batteryless 19µW MICS/ISM-Band Energy Harvesting Body Sensor Node SOC for EXG Applications. *IEEE J. Solid-State Circuits* **2013**, *48*, 199–213. [CrossRef]
49. Ramadass, Y.K.; Chandrakasan, A.P. A battery-less thermoelectric energy harvesting interface circuit with 35 mV startup voltage. *IEEE J. Solid-State Circuits* **2011**, *46*, 333–341. [CrossRef]
50. Photon Particle. Available online: https://www.particle.io/ (accessed on 11 November 2017).
51. Degrenne, N.; Buret, F.; Morel, F.; Adami, S.E.; Labrousse, D.; Allard, B.; Zaoui, A. Self-starting DC:DC Boost Converter for Low-Power and Low-Voltage Microbial Electric Generators. In Proceedings of the IEEE Energy Conversion Congress and Exposition (ECCE), Phoenix, AZ, USA, 17–22 September 2011; pp. 889–896.
52. Umaz, R.; Garrett, C.; Qian, F.; Li, B.; Wang, L. A Power Management System for Multianode Benthic Microbial Fuel Cells. *IEEE Trans. Power Electron.* **2017**, *32*, 3562–3570.